Chapter 5

DETECTION OF PEROXY INTERMEDIATES IN THE OXIDATION OF VOLATILE ORGANIC COMPOUNDS BY CHLORINE ATOMS

5.1 Introduction to chlorine atoms in the troposphere

Chlorine atoms (Cl) are extremely reactive species, oxidizing volatile organic compounds (VOCs) in the atmosphere at kinetic rates comparable to hydroxyl radicals (OH) and faster than ozone (O_3) and nitrate radicals (NO_3). Cl atoms, however, are lower in concentration (10^4 cm^{-3}) than other oxidants: [OH] = 10^6 cm^{-3}, [O_3] = 100 ppb, and [NO_3] = 50 ppt.[1] The impact of Cl atoms has therefore largely been restricted to coastal or marine regions. Sodium chloride (NaCl) from sea salt sprays react with the gas species dinitrogen pentaoxide (N_2O_5) and chlorine nitrate ($ClONO_2$) to form Cl photolytic precursors, nitryl chloride ($ClNO_2$) and chlorine (Cl_2):[2-7]

$$N_2O_5\ (g) + NaCl\ (s/aq) \rightarrow ClNO_2\ (g) + NaNO_3\ (s/aq) \qquad (5.1\ a)$$

$$ClNO_2\ (g) + h\nu \rightarrow Cl + NO_2 \qquad (5.1\ b)$$

$$ClONO_2\ (g) + NaCl\ (s/aq) \rightarrow Cl_2\ (g) + NaNO_3\ (s/aq) \qquad (5.2\ a)$$

$$Cl_2\ (g) + h\nu \rightarrow 2Cl \qquad (5.2\ b)$$

The heterogeneous chemistry of the reactions is not well-understood.[8-14] Models of the effect of $ClNO_2$ and Cl on the chemistry of coastal urban regions show increased ozone concentrations from rapid oxidant cycling.[15,16]

Recent studies indicate that chlorine levels may also be sufficiently high at mid-continental regions to impact local atmospheric chemistry.[17,18] Thornton, *et al.* observed $ClNO_2$ production in field studies at Boulder, Colorado (USA), 1400 km away from the nearest coastline.[17] From their models, they estimated 3.2-8.2 Tg yr^{-1} $ClNO_2$ production or 1.4-3.6 Tg yr^{-1} Cl atom formation from contiguous US regions. These estimates are comparable to global coastal and marine sources of $ClNO_2$ ~3.2 Tg yr^{-1}.[16]

A significant fraction of inland $ClNO_2$ production results from anthropogenic sources of Cl ions reacting with N_2O_5:[12,17-20]

$$N_2O_5\ (g) + Cl^-\ (aq) \rightarrow ClNO_2\ (g) + NO_3^-\ (aq) \qquad (5.1\ c)$$

Sources include emissions of chlorinated hydrocarbons such as trichloroethene (C_2HCl_3), tetrachloroethene (C_2Cl_4), dichloromethane (CH_2Cl_2), and trichloromethane ($CHCl_3$) from water treatment and paper facilities.[21-26] Chlorinated hydrocarbons can also be directly attacked by other atmospheric radicals to release Cl atoms.[1,27]

With prevalent Cl concentrations, the oxidation of VOCs by Cl atoms need to be better characterized. Similar to the oxidation of alkenes by NO_3, Cl addition to alkenes in the presence of oxygen leads to formation of substituted peroxy radicals:

$$R{=}R' + Cl \rightarrow R\text{-}R'(Cl) \qquad (5.3)$$

$$R\text{-}R'(Cl) + O_2 \rightarrow R\text{-}R'(Cl)O_2\ \text{(chloroalkenyl peroxy radical)} \qquad (5.4)$$

The addition of Cl to various alkenes has been studied.[28-48] Most works have focused on Cl addition to isoprene.[28,29,32,36,39,41-48] Isoprene has multiple sites of attack, resulting in formation of six Cl-isoprenyl peroxy radicals, three β-Cl-isoprenyl peroxy radicals and three δ-Cl-isoprenyl peroxy radicals (Fig. 5.1). Several experimental groups have measured the rate of Cl addition to isoprene (k_{298K}(isoprene + Cl) = 3-4 × 10^{-10} cm^3 $molec^{-1}$ s^{-1}) and have estimated branching ratios from end product analyses. One product, 1-chloro-3-methyl-3-buten-2-one (CMBO), in particular, has been cited as a possible tracer for chlorine chemistry in the atmosphere.[49]

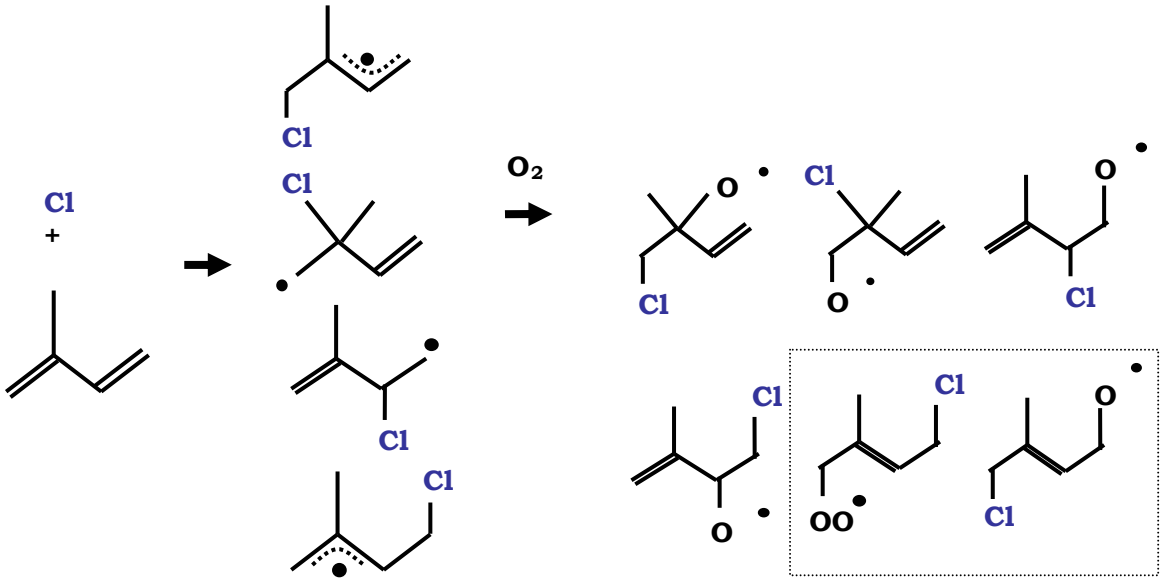

Figure 5.1. Schematics of Cl addition to isoprene in the presence of oxygen. Six structurally different Cl-isoprenyl peroxy radicals are formed. Four result from Cl addition to the β-C position, and two result from Cl addition to the δ-C position (dotted rectangle).

Molina *et al.* have done theoretical calculations on the formation of Cl-isopreny peroxy radicals and predict large yields for the δ-chloroisoprenyl peroxy radicals.[29] Unfortunately, there are no direct experimental studies on the branching ratios of the peroxy radicals. Hsin and Elrod have detected Cl-isoprenyl peroxy radicals with chemical ionization mass

spectrometry (CIMS) in their laboratory;[40] they were, however, unable to distinguish the different structural isomers. A method still needs to be developed to directly detect the Cl-isoprenyl peroxy radicals in the gas phase with a high degree of specificity.

Other biogenic VOCs contribute to the global atmospheric chemistry.[39,50,51] 2-methyl-3-buten-2-ol (MBO232) is emitted in large quantities from pine trees.[52-54] Addition of Cl to MBO232 leads to a peroxy radical with both Cl and OH substituents:

$$Cl + CH_2{=}CHC(CH_3)_2OH + O_2 \rightarrow CH_2(Cl)\text{-}CH(OO)C(CH_3)_2OH \qquad (5.5\ a)$$

$$\rightarrow CH_2(OO)\text{-}CH(Cl)C(CH_3)_2OH \qquad (5.5\ b)$$

While there have been kinetic studies on the Cl-oxidation of MBO232,[45,55-57] the double substituted peroxy radicals have never been directly observed. Thus, we outline in the next section our efforts to directly detect both the Cl-isoprenyl and Cl-MBO232 peroxy radicals in the gas phase.

5.2 Cl-peroxy radical detection

5.2.1 Background

Small chlorinated alkyl peroxy radicals have been detected in the ultraviolet (UV) region via the $\tilde{B} \leftarrow \tilde{X}$ transition by absorption methods. Samples include CH_2ClO_2, $CHCl_2O_2$, $ClCH_2CH_2O_2$, $CHCl_2CHClO_2$, $CHCl_2CCl_2O_2$, and $CCl_3CCl_2O_2$.[58-61] Larger chlorinated peroxy radicals, derivatives of methacrolein (MACR), methyl vinyl ketone (MVK), and alkenes have been detected with CIMS.[40,41] While both methods have

provided insight into the Cl-VOC oxidation chemistry, there are some limitations. With respect to UV studies, the observed spectra reveal strong and broad absorptions. Identification of the species is possible when the chemistry is limited to individual synthesis; however, it becomes difficult to distinguish the substituted peroxy radicals when multiple species are present. The CIMS studies also cannot distinguish between different structural isomers of the peroxy radical.

In the previous chapter, we detected substituted NO_3-peroxy radicals in the near-infrared (NIR) region via the $\tilde{A} \leftarrow \tilde{X}$ transition. Different structural isomers and conformers of the substituted peroxy radicals could be distinguished in the NIR spectra. Our group has already used this approach to detect Cl-alkyl peroxy radicals in the NIR region, including ethene, propene, butene, and butadiene derivatives.[62] We therefore use the same spectroscopic approach to directly detect the Cl-isoprenyl and Cl-MBO232 peroxy radicals in this work.

5.2.2 Preliminary scans of Cl-ethyl peroxy radical

The pulsed CRDS apparatus and optical cavity used in the study were identical to that described in the previous chapter for studies of the 2-NO_3-butyl peroxy radical. Only the chemistry or the gases used in the experiments differed. In our group's previous work on the Cl-alkyl peroxy radicals, we used photolysis of chlorine (Cl_2) at 308 nm as our Cl source. Chlorine molecules however react slowly with alkene species.

Oxalyl chloride (OxCl or $(ClC(O))_2$) has recently been demonstrated as a clean chlorine source:[63]

$$(ClC(O))_2 + h\upsilon \rightarrow 2\ Cl + 2\ CO \qquad (5.6)$$

As we had previously obtained a CRD spectrum of chloroethyl peroxy radical ($ClCH_2CH_2O_2$) in the NIR using Cl_2 photolysis, we conducted preliminary photolysis experiments with OxCl in the presence of ethene. Due to fragmentation of alkenes at 193 nm (Chapter 4), we conducted the photolysis experiments at 248 nm ($\sigma_{248\ nm}$(OxCl) = 2.7 × 10^{-19} cm^2).

OxCl (Sigma Aldrich) is a liquid at room temperature and solid at T < -5°C. We utilized methanol in a Neslab ULT 80 Chiller at T = -10°C for our bath instead of the standard salt water/liquid nitrogen bath, as OxCl reacts violently with water. In fact, excess OxCl from experiments was disposed in the hood by slow addition of water droplets. Under regular flow conditions, the vapor pressure of solid OxCl was ~1.5 Torr. Photolysis experiments with only OxCl in the ringdown cell showed no absorption in the 7000-7600 cm^{-1} region.

Experiments were run at total pressure 40 Torr, with OxCl at 1.5 Torr, ethene (Matheson) at 1.5 Torr, zero grade air at 30 Torr, and N_2 purge for the CRD mirrors at 7 Torr. The excimer was operated at 5 Hz to insure the gases had time to flush the cell between each excimer fire. Unlike NO_3-ethene oxidation, Cl attacks ethene rapidly. Within 10 μs, all the Cl atoms are consumed. We therefore delayed our NIR laser by 10-50 μs for peroxy radical detection.

The preliminary CRD spectrum of photolysis of OxCl in the presence of ethene at 248 nm is shown in Fig. 5.2, along with our previously observed spectrum of Cl-ethyl peroxy radical from the photolysis experiments of Cl_2 at 308 nm. The two spectra are identical. Similarly to how we checked the consistency of the NO_3-peroxy radical concentrations with the limiting reactant NO_3 concentrations (Chapter 4),

we compare here the concentration of Cl-ethyl peroxy radical with Cl atom concentrations.

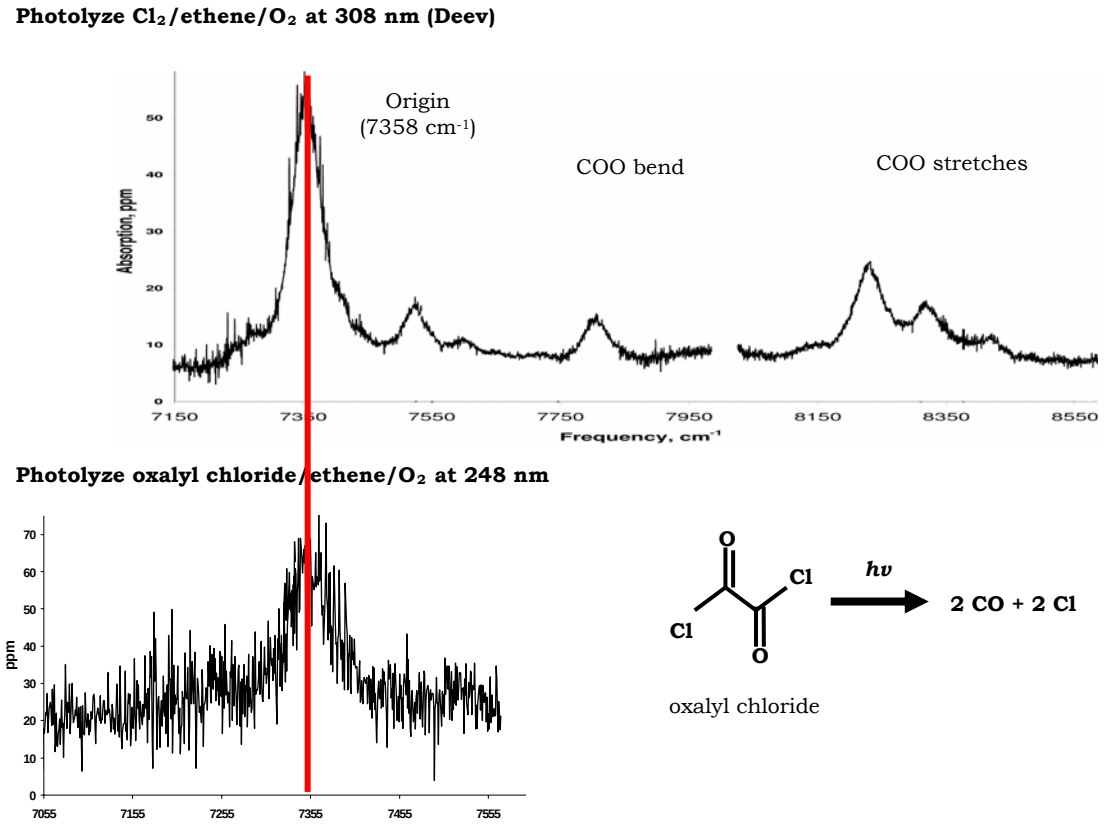

Figure 5.2 Preliminary CRD spectrum of the $\tilde{A} \leftarrow \tilde{X}$ transition of Cl-ethyl peroxy radical in the NIR region (bottom). The spectrum was obtained from photolysis of oxalyl chloride at 248 nm in the presence of ethene and oxygen. We compared the spectrum to the CRD spectrum of Cl-ethyl peroxy radcial obtained from photolysis of chlorine at 308 nm in the presence of ethene and oxygen (top). The two spectra are identical.

Given σ_{NIR} ($ClCH_2CH_2O_2$)~10^{-20} cm^2 and the parameters of our medium-sized photolysis cell, from the observed peak Cl-ethyl peroxy radical absorption (~45 ppm), we estimate [$ClCH_2CH_2O_2$]~3 × 10^{14} molec cm^{-3}. At excimer powers of 100 mJ/pulse at 248 nm, we generate chlorine concentrations:

$$[Cl] = [OxCl] \times \sigma_{248nm}(OxCl) \times \frac{\#\ photons\ /\ pulse}{area} \times 2$$
$$= (1.5 \times 3 \times 10^{16}) \times (2.7 \times 10^{-19}) \times \frac{10^{18} * 0.1}{12.7 \times 0.5} \times 2 \qquad (5.7)$$
$$= 3.8 \times 10^{14}\ \text{molec cm}^{-3}$$

The consistency of the two values indicates that OxCl photolysis in the presence of alkene directly leads to Cl-peroxy radical formation. The signal-to-noise (S/N) of our spectrum could be further improved by optimizing the excimer and optical cavity alignment. The experiment confirmed that we could use OxCl as our Cl source for the remaining Cl-peroxy radical experiments.

5.2.3 Cl-isoprenyl peroxy radical detection

Preliminary results

Due to the atmospheric significance of isoprene, we began our studies with detection of Cl-isoprenyl peroxy radicals. Isoprene (Sigma Aldrich) is a liquid at very low temperatures. It is also very sensitive to light. We therefore put 5 mL of isoprene in a bubbler and wrapped the container with aluminum foil. The wrapped bubbler was then placed in a dry ice acetone bath (T = -60 °C) and covered with a black blanket. Zero grade air was passed through a molecular sieve before being used as carrier gases for both the isoprene and oxalyl chloride samples in the experiments. As the peroxy radical scan will eventually cover a large wavelength region (>1000 cm^{-1} using multiple laser dyes), we recorded for reproducibility the flow rates and pressures for each reactant gas (Fig. 5.3). Experiments were run at total pressure 40 Torr, with zero grade air carrier for OxCl at 15 Torr, OxCl at 1.5 Torr, zero grade air carrier for isoprene at 15 Torr, isoprene at 1.5 Torr, and N_2 purge at 10 Torr.

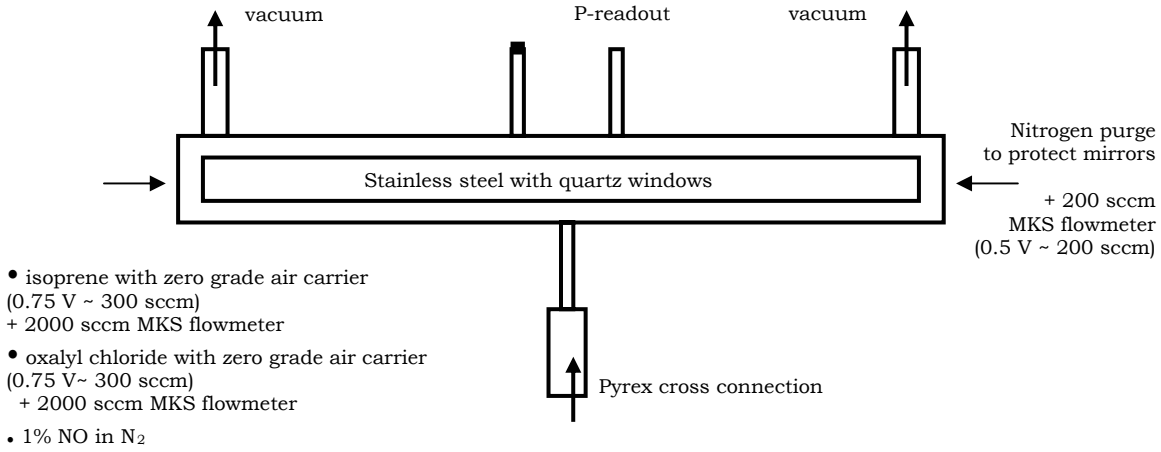

Figure 5.3. Schematic of ringdown cell for isoprene+ OxCl experiments. The gas flow conditions are provided in the figure.

Neither the isoprenyl nor other substituted isoprenyl peroxy radicals have been observed in the NIR region, and *ab inito* calculations on the origin band frequency have not been done for such a large peroxy radical system. We therefore relied on our group's previous CRD study on the $\tilde{A} \leftarrow \tilde{X}$ transitions of resultant peroxy radicals from oxidation of 1,3-butadiene by Cl to estimate the scanning region for the Cl-isoprene oxidation study. The observed origin band is a broad absorption from 7200-7600 cm^{-1} with two major bumps at 7500 and 7600 cm^{-1} for different isomers of the radical. We therefore conducted preliminary experiments in the 7200-7600 cm^{-1} region using the DCM dye and Layertec 1390 nm mirrors. Scans were collected at 0.4 cm^{-1} step size for the excimer on and off with isoprene/OxCl or isoprene alone in the ringdown cell. Due to fast Cl kinetics, we primarily collected spectra 10 μs after excimer fire.

The preliminary CRD spectrum of Cl-isoprenyl peroxy radical was obtained by subtraction of the isoprene/OxCl scans with the excimer on and off (Fig. 5.4). The absorptions in the spectrum resemble that of Cl-butadienyl peroxy radical, with a strong broad absorption between 7250-

7700 cm^{-1} and multiple bumps at 7450 cm^{-1} and 7650 cm^{-1}. The difference between the isoprene scans with the excimer on and off showed a flat line, indicating that the absorptions observed in Fig. 5.4 were not from photolysis of isoprene. The absorptions were also not from isoprene itself, which has C-H overtone absorptions in the NIR region (Fig. 5.5).

We conducted additional experiments to confirm whether the absorptions belonged to the Cl-isoprenyl peroxy radical. As the lifetime of peroxy radicals is on the order of milliseconds, we delayed our NIR probe with respect to the excimer fire and observed the absorptions decay over time. The absorptions could be scaled such that they were identical, indicating that all absorptions belonged to the same species. We also injected nitric oxide (NO) into the cell, along with isoprene and OxCl, during the photolysis experiment, as NO should react with the peroxy radicals rapidly. We consequently observed rapid decay of the absorptions in the time-resolved spectra.

The preliminary experiments suggest that the observed absorptions can be assigned to the $\tilde{A} \leftarrow \tilde{X}$ transition of Cl-isoprenyl peroxy radical. In the last chapter, we discussed how peroxy radicals have signature torsional absorptions 500 cm^{-1} and 1000 cm^{-1} to the blue of the origin, corresponding to the COO bend and OO stretch, respectively. We therefore plan to scan 1000 cm^{-1} to the blue of the current spectral range for spectroscopic confirmation of the peroxy radical assignment.

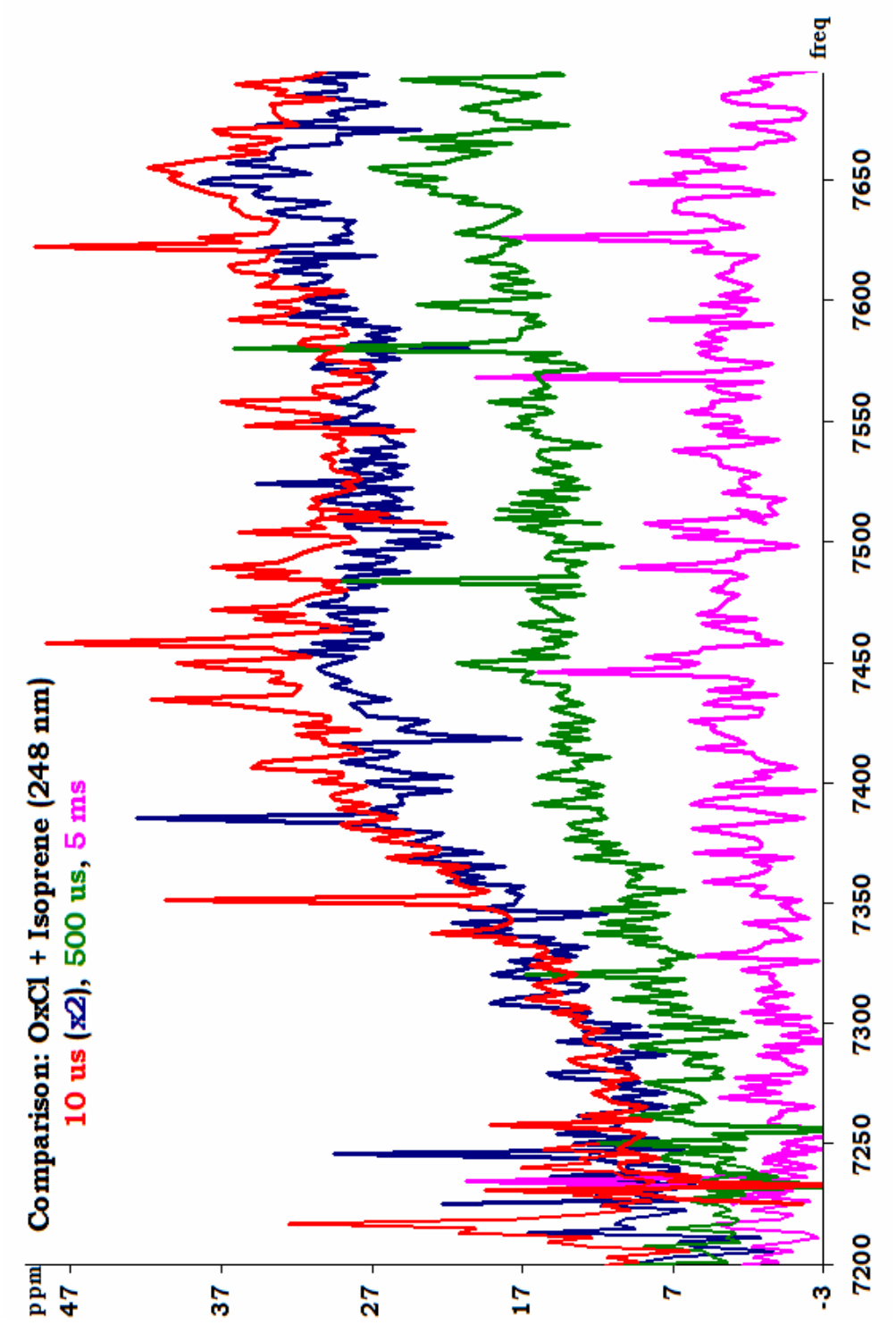

Figure 5.4. Preliminary CRD spectra of Cl-isoprenyl peroxy radical in the 7200-7700 cm^{-1} region, collected at various delay times after excimer fire (t = 10 μs, 500 μs, and 5 ms). The absorption signal decays, as the peroxy radicals self-react.

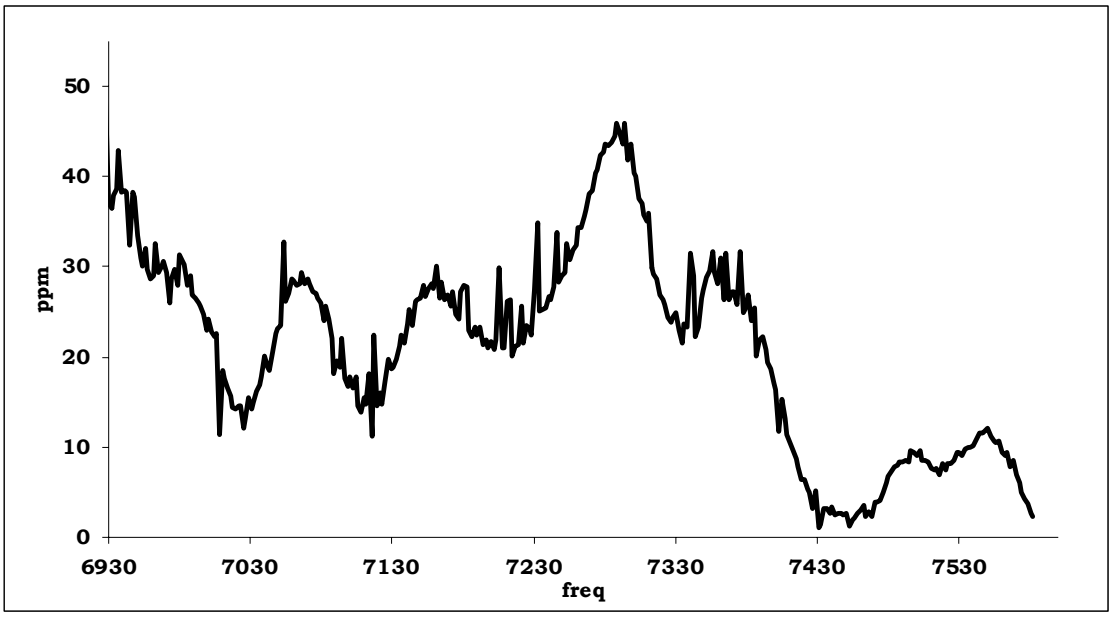

Figure 5.5. CRD spectrum of isoprene in the 6930-7550 cm^{-1} region. We subtracted a 10 ppm offset in the figure. There are several strong peaks in the 7030-7430 cm^{-1} region. These spectral features were not observed in the photolysis experiment with OxCl and isoprene, confirming that absorption contributions from isoprene were effectively removed during subtraction of the excimer on/off for CRD experiments (Fig. 5.4).

Large scan for Cl-peroxy radical

We divide the large scan (7200-8700 cm^{-1}) into smaller segments, as we are limited by the wavelength range of the laser dyes (Chapter 2). Successive spectra must be scaled appropriately such that spectral intensities can be directly compared. One option is to use absorption features in overlapping spectral regions to scale the spectra. Ideally, the spectra should be scaled by the concentration of Cl-isoprenyl peroxy radical generated in each experiment. In our study of the oxidation of 2-butene by NO_3, the concentration of NO_3 was the limiting reactant for 2-NO_3-butyl peroxy radical formation. Thus, we used CRD spectra of NO_3 to scale all collected spectra. We could similarly use the measurement of Cl atoms to directly estimate the concentration of Cl-isoprenyl peroxy radical formation.

Neither OxCl nor the Cl atom have absorptions in the NIR region. We could measure the excimer power and estimate the concentration of Cl atom formation from the vapor pressure of OxCl and absorption cross section of OxCl at 248 nm. A more accurate measurement would be spectroscopic quantification of a species related directly to Cl atom concentrations under similar gas flow conditions as the Cl-isoprene oxidation experiments. We therefore propose to use formation of ethyl peroxy radicals as a means to measure the Cl concentrations in the experiment.

The oxidation of alkanes by radicals proceeds by hydrogen abstraction and forms peroxy radicals in the presence of oxygen. For the simplest alkanes:[64]

$Cl + CH_4 \rightarrow CH_3 + HCl$ (5.8 a)

$k_{298\,K}$ ($Cl + CH_4$) = 1.0 x 10^{-13} cm^3 $molec^{-1}$ s^{-1} (5.8 b)

$CH_3 + O_2 \rightarrow CH_3O_2$ (methyl peroxy radical) (5.9)

$Cl + C_2H_6 \rightarrow CH_3CH_2 + HCl$ (5.10 a)

$k_{298\,K}$ ($Cl + C_2H_6$) =5.7 x 10^{-11} cm^3 $molec^{-1}$ s^{-1} (5.10 b)

$CH_3CH_2 + O_2 \rightarrow CH_3CH_2O_2$ (ethyl peroxy radical) (5.11)

Both methyl and ethyl peroxy radicals are produced 1:1 with respect to the Cl atoms. CRD spectra of the $\tilde{A} \leftarrow \tilde{X}$ transition of both peroxy radicals have been published and show distinct spectral features in the 7200-8700 cm^{-1} region.[65-67] We chose to use ethyl peroxy radicals in this work, as Cl addition to ethane proceeds faster than addition to methane. The same chemical approach has been used to determine the absorption cross section of ethyl peroxy radical in the NIR region. Melnik, *et al.* used a dual wavelength CRD spectrometer to detect both the ethyl peroxy

radical and HCl production simultaneously.[68] As the cross sections for HCl lines are well-known, they determined a peak absorption cross section for ethyl peroxy radical at 7596 cm^{-1}, $\sigma_{NIR}(CH_3CH_2O_2)$ = 5.29(20) × 10^{-21} cm^2. Thus, we use the spectra of ethyl peroxy radical to not only scale the overlapping spectra for Cl-isoprene oxidation but to also determine the exact concentration of Cl-isoprenyl peroxy radicals observed in the experiments.

Preliminary experiments on the detection of ethyl peroxy radicals were conducted with the pulsed CRD apparatus. We maintained similar gas flow conditions as our Cl-isoprene oxidation experiments. The only major difference was the replacement of the isoprene source with ethane (Matheson). The excimer was operated at 5 Hz and the NIR probe laser was delayed 10-50 μs after the excimer fire. We collected scans of the OxCl/ethane mixture with the excimer on and off and obtained a CRD spectrum of the ethyl peroxy radical from the difference between the two scans (Fig. 5.6). The spectral features were consistent with previously published NIR spectra of the ethyl peroxy radical.

The gas lines for isoprene (or specifically the zero grade air carrier for isoprene) and ethane are interchangeable such that ethyl peroxy radical scans can be run before and after every Cl-isoprene oxidation experiment. Thus, we are now prepared to conduct our wide range scans on the Cl-isoprene oxidation system.

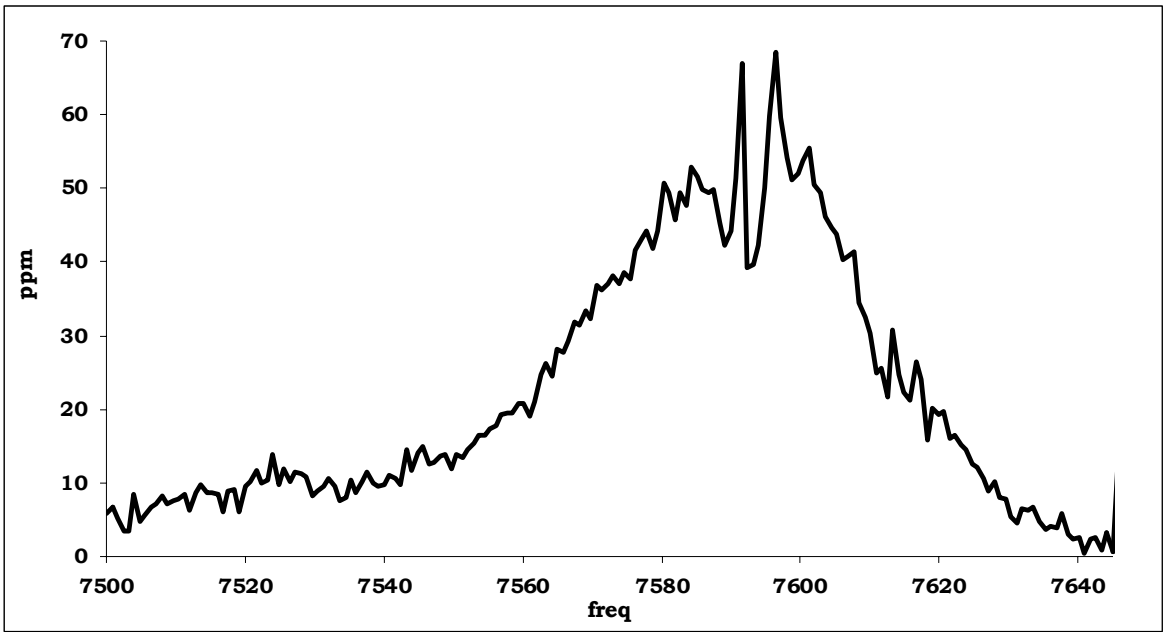

Figure 5.6. Preliminary spectrum of the $\tilde{A} \leftarrow \tilde{X}$ transition of ethyl peroxy radical in the 7500-7650 cm^{-1} region. The concentration of ethyl peroxy radicals is related directly to the concentration of Cl atoms generated in the photolysis cell. The Cl atoms further determine the concentration of Cl-isoprenyl peroxy radicals formed during the oxidation experiments.

5.2.4 Cl-MBO232 peroxy radical detection

Preliminary results

In addition to the low-lying electronic transitions, OH vibrational overtones have absorptions in the NIR region. We expect to observe both the origin of the $\tilde{A} \leftarrow \tilde{X}$ transition and the OH overtone of Cl-MBO232 peroxy radical in the NIR region. We outline methods to distinguish the two transitions in the spectra.

With respect to the $\tilde{A} \leftarrow \tilde{X}$ transition, addition of Cl to MBO232 results in two structural isomers, I (rxn 5.5 a) and II (rxn 5.5 b) (Fig. 5.7). Peroxy isomer I resembles the 3-methyl-2-butyl peroxy radical, while peroxy isomer II resembles the 3-methylbutyl peroxy radical. NIR spectra of the $\tilde{A} \leftarrow \tilde{X}$ transitions for both methylbutyl peroxy radicals

have been published.[69] For the 3-methyl-2-butyl peroxy radical, three different conformers were observed with origin bands at 7318 cm^{-1}, 7490 cm^{-1}, and 7549 cm^{-1}. The most intense absorption was located between 7500-7620 cm^{-1} with two sharp bumps for two of the conformers. For the 3-methylbutyl peroxy radical, three conformers were observed with origin bands at 7361 cm^{-1}, 7551 cm^{-1}, and 7620 cm^{-1}. The most intense absorption was between 7200-7800 cm^{-1}, with a very sharp rise to the 7620 cm^{-1} peak.

The addition of both Cl and OH substituents should shift the origins of the conformers to the red. The shape however should be very similar. We should be able to identify the absorptions arising from the Cl-MBO232 peroxy radical from spectral comparisons. We can then scan 500 cm^{-1} and 1000 cm^{-1} to the blue of the observed origin band frequencies to detect the signature torsional absorptions of peroxy radicals for spectroscopic confirmation of the assignments.

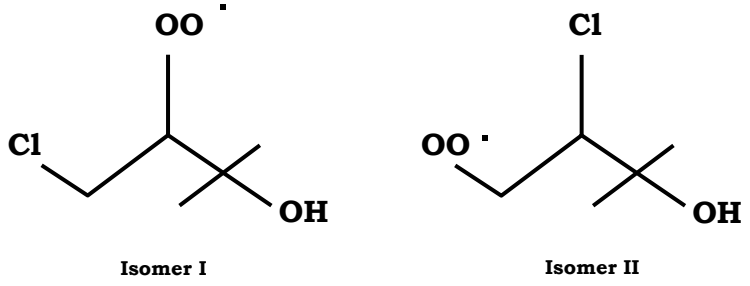

Figure 5.7. The two structural isomers of Cl-MBO232 peroxy radical.

With respect to the OH overtone, most OH stretches are in the 3500 cm^{-1} region with overtones in the 7000 cm^{-1} region. The mid-IR and NIR spectra of ethanol and Cl-ethanol were compared and found to be very similar in band shape and position.[70] Thus, as long as the Cl substituent does not directly affect the OH stretch, the effect on the

absorptions should be minimal. The parent compound MBO232 has an OH overtone absorption in the NIR region. The OH overtones for both isomers of Cl-MBO232 peroxy radicals should have very similar absorptions. Thus, we obtain a CRD spectrum of MBO232 as a reference. The OH absorption should be to the red of the $\tilde{A} \leftarrow \tilde{X}$ transitions of the peroxy radicals. We may not be able to observe the weak peroxy radical conformer absorption in the 7300 cm^{-1} region, but we should be able to observe the conformer absorptions in the 7500-7700 cm^{-1} region without much spectral interference.

Experiments on the Cl oxidation of MBO232 were conducted using the same pulsed CRDS apparatus and gas flow conditions as described in the previous section. Only the isoprene sample with replaced with MBO232 (Sigma Aldrich). MBO232 is a liquid at room temperature. We pipetted 5 mL of MBO232 into a bubbler and placed it in a methanol chiller bath (T ~ -10°C). Experiments were typically run with 1.5 Torr vapor pressure of MBO232. Scans were taken at 0.4 cm^{-1} step size with the excimer operating at 5 Hz and the NIR probe delayed 10 μs after chemical initiation.

Preliminary CRD spectra of Cl-MBO232 peroxy radical were obtained in the 7150-7600 cm^{-1} region from subtraction of scans collected with the excimer on and off for OxCl/MBO232 in the ringdown cell (Fig. 5.8). A CRD spectrum was also obtained for MBO232 (Fig. 5.9). The absorptions observed in the two spectra (Fig. 5.8 and Fig. 5.9) are very different, especially in the 7450-7600 cm^{-1} region. While more experiments are needed to confirm that the absorptions in the latter region belong to the $\tilde{A} \leftarrow \tilde{X}$ transition of the peroxy radicals, the preliminary results look very promising. It may be worthwhile to extend the CRD studies to Cl-oxidation of 3-methyl-1-butene to examine the effect of the OH

substituent on the origin frequency of $\tilde{A} \leftarrow \tilde{X}$ transition and better assign which bands belong to the OH overtone in the current spectra.

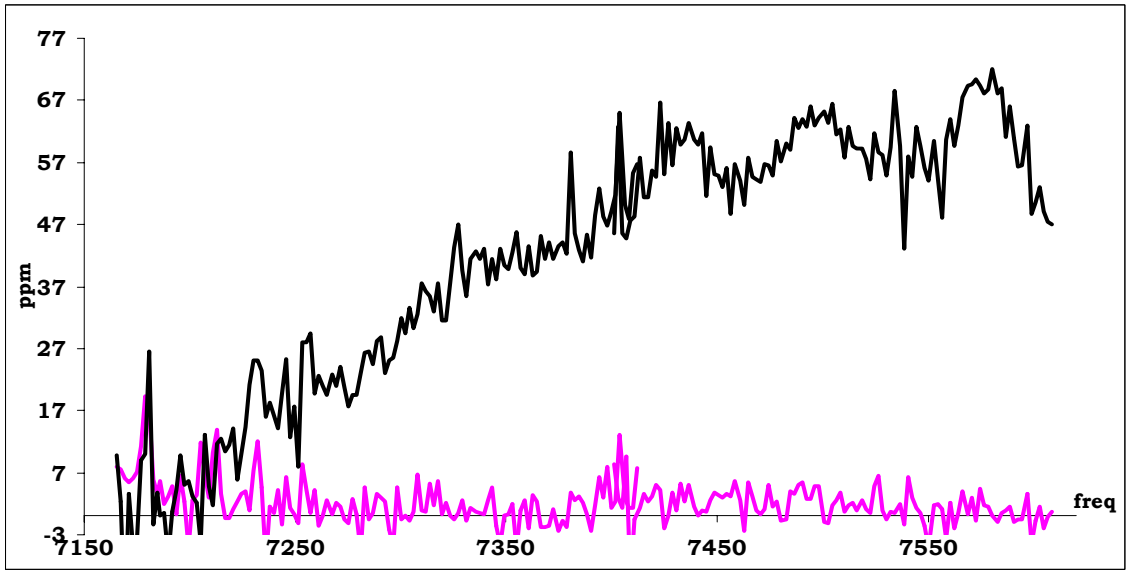

Figure 5.8. Preliminary CRD spectra of Cl-MBO232 peroxy radical in the 7150-7600 cm^{-1} region. The scans were collected at t =10 μs (black) and t = 2 ms (pink) after the excimer fire. The peroxy radical disappeared over time from self-reaction.

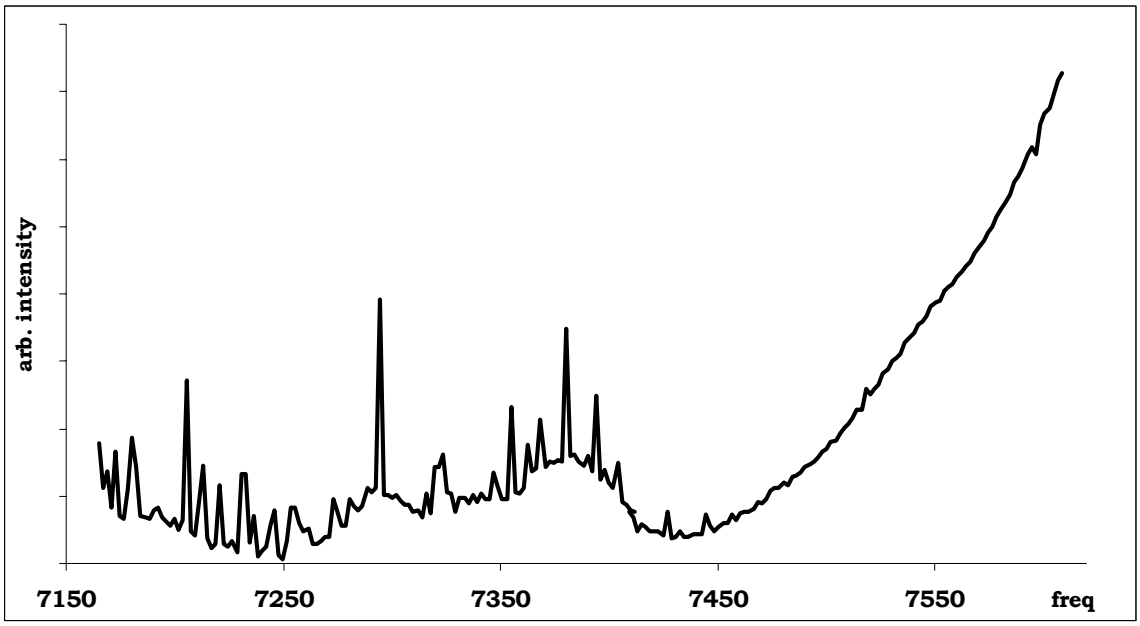

Figure 5.9. Preliminary CRD spectrum of MBO232 in the 7150-7600 cm^{-1} region. The spectrum has not been background-subtracted. The spectral rise at 7450 cm^{-1} is therefore from the reflectivity of the CRD mirrors. Problems with the laser power prevented scans to the red of 7150 cm^{-1}. The OH overtone should be around 7000 cm^{-1}.

5.3 Cl-peroxy radical kinetics

5.3.1 Background

We have thus far discussed the detection of substituted peroxy radicals. Detection of the radicals allows us to examine the kinetics of the substituted peroxy radicals. In Chapter 1, we outlined two different environments for peroxy radical kinetics: high and low NO_x conditions. Under high NO_x conditions, the reaction between the peroxy radicals and nitric oxide (NO) dominates. Under low NO_x conditions, the reaction between the peroxy radicals with hydroperoxy radical HO_2 and other peroxy radicals dominates. For substituted peroxy radicals, most of these rates of reaction have never been measured.

For Cl-peroxy radicals, the self reaction rates for a few species have been measured using UV absorption spectroscopy: $CHCl_2CHClO_2$, $CHCl_2CCl_2O_2$, $CCl_3CCl_2O_2$, CH_2ClO_2, $CHCl_2O_2$, and $ClCH_2CH_2O_2$. Self reactions rates vary from from k_{298K} ($ClRO_2$ + $ClRO_2$) = 3.6-8.6 × 10^{-12} cm^3 $molec^{-1}$ s^{-1}.[58,59,61] For comparison, self-reaction rates of methyl and ethyl peroxy radicals have been measured, k_{298K} (CH_3O_2+CH_3O_2) = 3.5 × 10^{-13} cm^3 $molec^{-1}$ s^{-1} and k_{298K} ($CH_3CH_2O_2$+$CH_3CH_2O_2$) = 6.8 × 10^{-14} cm^3 $molec^{-1}$ s^{-1}, respectively.[64] Cl addition significantly increases the rate of self-reaction:

$ClRO_2$ + $ClRO_2$ → Products (5.12 a-b)

k_{298K} ($ClRO_2$ + $ClRO_2$) = 3.6-8.6 × 10^{-12} cm^3 $molec^{-1}$ s^{-1}

RO_2 + RO_2 → Products (5.13 a-b)

k_{298K} (RO_2 + RO_2) = 0.68-3.5 × 10^{-13} cm^3 $molec^{-1}$ s^{-1}

There has been one measurement for the reaction between the Cl-ethyl peroxy radical ($ClCH_2CH_2O_2$) and HO_2: k_{298K} ($ClCH_2CH_2O_2 + HO_2$)= 1.4×10^{-11} cm^3 $molec^{-1}$ s^{-1}.[58] The reaction rate between the ethyl peroxy radical and HO_2 has been measured to be k_{298K} ($CH_3CH_2O_2 + HO_2$) = 8×10^{-12} cm^3 $molec^{-1}$ s^{-1}.[64] The rate of reaction is again increased by Cl addition:

$ClCH_2CH_2O_2 + HO_2 \rightarrow$ Products (5.14 a-b)

k_{298K} ($ClCH_2CH_2O_2 + HO_2$)= 1.4×10^{-11} cm^3 $molec^{-1}$ s^{-1}

$CH_3CH_2O_2 + HO_2 \rightarrow$ Products (5.15 a-b)

k_{298K} ($CH_3CH_2O_2 + HO_2$) = 8×10^{-12} cm^3 $molec^{-1}$ s^{-1}

Finally, there have been CIMS studies by the Elrod group on the reaction rate between NO and Cl-alkenyl and Cl-MACR/MVK peroxy radicals.[40,41] Measured rates range from k_{298K} ($ClRO_2 + NO$) = 0.84-1.17 $\times 10^{-11}$ cm^3 $molec^{-1}$ s^{-1}. Reaction rates for methyl and ethyl peroxy radicals with NO are k_{298K} ($CH_3O_2 + NO$) = 7.7×10^{-12} cm^3 $molec^{-1}$ s^{-1} and k_{298K} ($CH_3CH_2O_2 + NO$) = 8.7×10^{-12} cm^3 $molec^{-1}$ s^{-1}, respectively.[64] Cl addition appears to have less effect on the reaction rates:

$ClRO_2 + NO \rightarrow$ Products (5.16 a-b)

k_{298K} ($ClRO_2 + NO$) = 8.4-11.7 $\times 10^{-12}$ cm^3 $molec^{-1}$ s^{-1}

$RO_2 + NO \rightarrow$ Products (5.17 a-b)

k_{298K} ($RO_2 + NO$) = 7.7-8.7 $\times 10^{-12}$ cm^3 $molec^{-1}$ s^{-1}

A handful of theoretical works have examined the effect of Cl addition on the reaction rates. King and Thompson examined singly occupied molecule orbitals (SOMO) of reactant species and determined that peroxy

radicals derived from halogenated alkenes had faster rate constants for reaction with NO relative to reaction with HO_2.[71] There are not enough measurements of the reaction rate between Cl-peroxy radical and HO_2 to verify the theory. Kosmas, *et al.* performed *ab initio* and density functional calculations on the reaction between halogenated methyl peroxy radicals and NO and found that the increased attractive character of the potential energy surface, along with the increased exothermicity of the reactions, contributed to higher rates of reaction between halogenated methyl peroxy radical and NO than methyl peroxy radicals and NO.[72] The available experimental data, however, indicates that the rates of reaction between halogenated and non-halogenated species with NO are very similar. More experimental work is needed.

To date, despite the significance of isoprenyl peroxy radicals in the atmosphere, the previously mentioned CIMS study is the only direct measurement of the rate of reaction between Cl-isoprenyl peroxy radical and NO. There has been no direct measurements on the reaction rates between Cl-MBO232 peroxy radicals and other atmospheric species. We therefore propose to measure the following rates of reaction for the Cl-isoprenyl and MBO232 peroxy radicals: the rate of self-reaction, the rate of reaction with NO, and the rate of reaction with HO_2.

Reproducibility and fine experimental control are key factors in kinetic measurements. Before we begin the complicated kinetic measurements, we need to conduct control experiments to better characterize the apparatus. We chose to examine the kinetics of ethyl peroxy radical for this purpose.

5.3.2 Kinetics of the ethyl peroxy radical

The kinetics of ethyl peroxy radicals have been studied in great detail.[64,73] We generate ethyl peroxy radicals via H-abstraction by Cl atoms from ethane (Fig. 5.6). As the peak cross section for the ethyl peroxy radical has been measured in the NIR, we can measure absolute concentrations of ethyl peroxy radicals for the kinetic experiments. We use the kinetic modeling program Kintecus (version 4.0)[74] to model the ethyl peroxy radical chemistry under both high and low NO_x conditions. The simulated decays of the ethyl peroxy radical can be directly compared to the measured signal decays of the ethyl peroxy radical from the pulsed CRDS experiments. We outline the CRD studies below.

Testing wall reactions via self-reaction experiments

A major concern for kinetic experiments is wall reactions. Products stick to the cell walls and react with the intermediates of interest. We have worked on coating the ringdown cell with halocarbon wax and Fluoropel to minimize heterogeneous reactions. To quantitatively test the conditions of the cell, we measure the rate of self-reaction for the ethyl peroxy radical:

$$2\ CH_3CH_2O_2 \rightarrow \text{products} \qquad (5.18\ a)$$

$$-\frac{\partial[CH_3CH_2O_2]}{\partial t} = k[CH_3CH_2O_2]^2$$
$$\Rightarrow \frac{1}{[CH_3CH_2O_2(t)]} - \frac{1}{[CH_3CH_2O_2(0)]} = kt \qquad (5.18\ b)$$

The Cl + ethane kinetics model is shown in Table 5.1. Simulations were run under experimental conditions: T = 298 K and P = 50 Torr, with $[C_2H_6]_0 = 3 \times 10^{16}$ molec cm^{-3} (~1 Torr), $[Cl]_0 = 5 \times 10^{13}$ molec cm^{-3}, and $[O_2]_0 = 50 \times 3 \times 10^{16}$ molec cm^{-3}. The concentrations of the ethyl peroxy radical are plotted with respect to time in Fig. 5.10. When there is no external reactant, the concentration of the ethyl peroxy radical decreases only by 10% over a 10-ms timeframe. Deviations in the observed decay from the model would most likely be from wall loss.

Kinetics model for Cl + ethane

Reaction equations	**Rates of reaction at T = 298 K [cm^3 molec^{-1} s^{-1}]**
$C_2H_6 + Cl \rightarrow C_2H_5 + HCl$	5.7×10^{-11}
$C_2H_5 + O_2 + M \rightarrow C_2H_5O_2$	1.1×10^{-12} at M = 50 Torr, 760 Torr
$\rightarrow C_2H_4 + HO_2$	$< 2 \times 10^{-14}$
$2\ C_2H_5O_2 \rightarrow 2\ C_2H_5O + O_2$	$2.3(1.1) \times 10^{-14}$*, 7.3×10^{-14}**
$\rightarrow C_2H_5OH + CH_3CHO + O_2$	$1.0(0.1) \times 10^{-13}$*, 3.6×10^{-14}**, 6.8×10^{-14}
$\rightarrow C_2H_5O_2C_2H_5 + O_2$	
$C_2H_5O + O_2 \rightarrow HO_2 + CH_3CHO$	1.0×10^{-14}
$2\ HO_2 \rightarrow H_2O_2 + O_2$	1.7×10^{-12}*
$C_2H_5O_2 + HO_2 \rightarrow C_2H_5OOH + O_2$	$5.5(0.4) \times 10^{-12}$*, 8×10^{-12}
$2\ C_2H_5 \rightarrow C_4H_{10}$	$1.99(0.44) \times 10^{-11}$**
$C_2H_5O_2 + C_2H_5O \rightarrow C_2H_5OOH + CH_3CHO$	$1.5(0.7) \times 10^{-11}$*

Table 5.1. Kinetics model for Cl + ethane. References for rates of reaction: unmarked = ref[64], * = ref[75], and ** = ref[76]

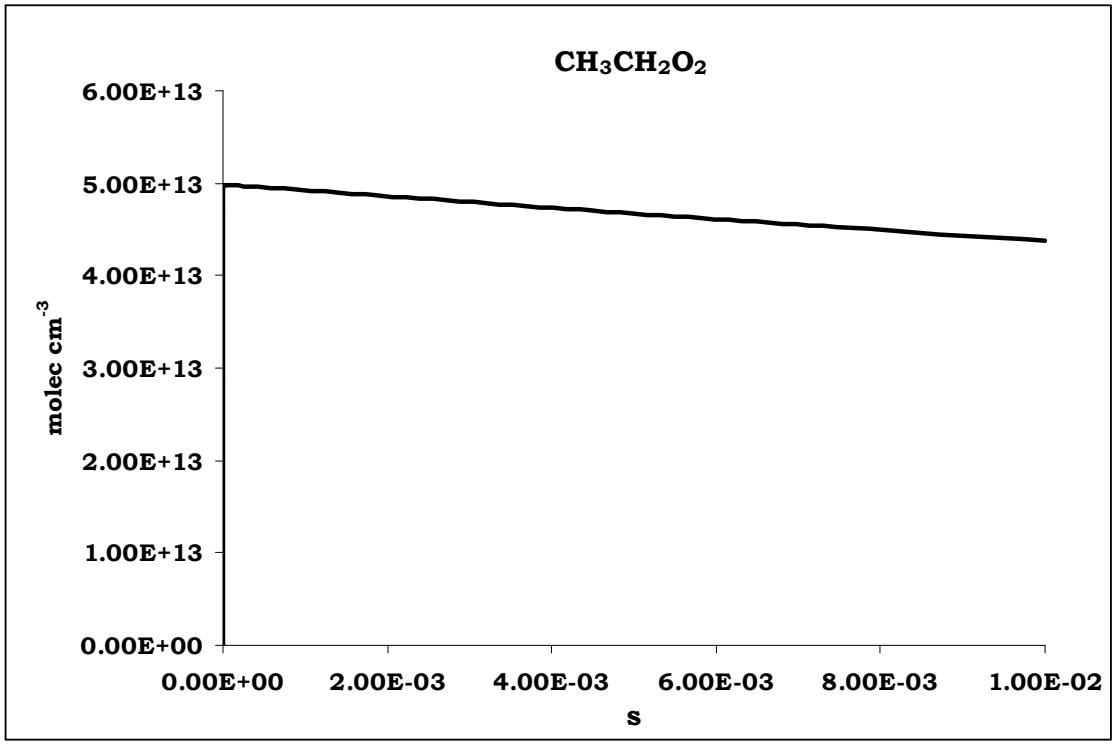

Figure 5.10. Concentrations of the ethyl peroxy radical using the kinetics model from Table 5.1. The initial reactant concentrations are: $[C_2H_6]_0$ = 3 × 10^{16} molec cm^{-3} (1 Torr), $[Cl]_0$ = 5 × 10^{13} molec cm^{-3}, and $[O_2]_0$ = 50 × 3 × 10^{16} molec cm^{-3}.

Kinetic experiments with NO

A mass flow controller (Edwards, 100 sccm) is added to the NO (1% Matheson) line for fine control and reproducibility. The pressure readout is used to relate the flow rate with the concentration of NO added to the ringdown cell. Experiments are run under pseudo-first-order conditions, such that the concentrations of NO remain constant during the experiment, $[NO] = [NO]_0$.

$$CH_3CH_2O_2 + NO \rightarrow CH_3CH_2O + NO_2 \qquad (5.19\ a)$$

$$-\frac{\partial[CH_3CH_2O_2]}{\partial t} = k[NO][CH_3CH_2O_2] \simeq k_{obs}[CH_3CH_2O_2]$$
$$\Rightarrow [CH_3CH_2O_2(t)] = [CH_3CH_2O_2(0)] \times e^{-k_{obs}t} \qquad (5.19\ b)$$

where $k_{obs} = k[NO]_0$.

The reactions listed in Table 5.2 are added to the previous kinetics model for simulations. The concentration of the ethyl peroxy radical are re-plotted with respect to time (Fig. 5.11).

Kinetics model for Cl + ethane with NO	
Reaction formulas	**Rates of reaction at T = 298 K [cm^3 $molec^{-1}$ s^{-1}]**
$C_2H_5O_2 + NO \rightarrow C_2H_5O_2NO$	8.7×10^{-12}
$C_2H_5O + NO + M \rightarrow C_2H_5ONO$	4.4 & 7×10^{-11} at [M] = 50 & 760 Torr
$C_2H_5O + NO_2 + M \rightarrow C_2H_5ONO_2$	2.5 & 7×10^{-11} at [M] = 50 & 760 Torr
$HO_2 + NO \rightarrow NO_2 + OH$	8.1×10^{-12}
$HO_2 + NO_2 + M \rightarrow HO_2NO_2$	0.21 & 1.0×10^{-12} at [M] = 50 & 760 Torr
$OH + OH \rightarrow H_2O + O$	1.8×10^{-12}
$+ M \rightarrow H_2O_2$	0.84 & 6.0×10^{-12} at [M] = 50 & 760 Torr
$OH + HO_2 \rightarrow H_2O + O_2$	1.1×10^{-10}
$OH + H_2O_2 \rightarrow H_2O + HO_2$	1.8×10^{-12}
$OH + NO + M \rightarrow HONO$	0.89 & 7.1×10^{-12} at [M] = 50 & 760 Torr
$OH + NO_2 + M \rightarrow HNO_3$	0.19 & 1.0×10^{-11} at [M] = 50 & 760 Torr
$\rightarrow HOONO$	0.13 & 1.7×10^{-12} at [M] = 50 & 760 Torr
$OH + HO_2NO_2 \rightarrow$ Product	4.6×10^{-12}
$OH + C_2H_6 \rightarrow H_2O + C_2H_5$	2.4×10^{-13}
$OH + C_2H_5ONO_2 \rightarrow$ Product	2×10^{-13}
$OH + HCl \rightarrow H_2O + Cl$	8×10^{-13}
$Cl + O_2 + M \rightarrow ClOO$	0.33 & 4.9×10^{-14} at [M] = 50 & 760 Torr

Table 5.2. Kinetics model for Cl + ethane with NO. The model also includes all reactions from Table 5.1. OH is formed late in the reaction after HO_2 concentrations become relevant. While they are included in the model (in rectangle box), they are not expected to affect the ethyl peroxy radical yields significantly. Rates of reaction from ref [64].

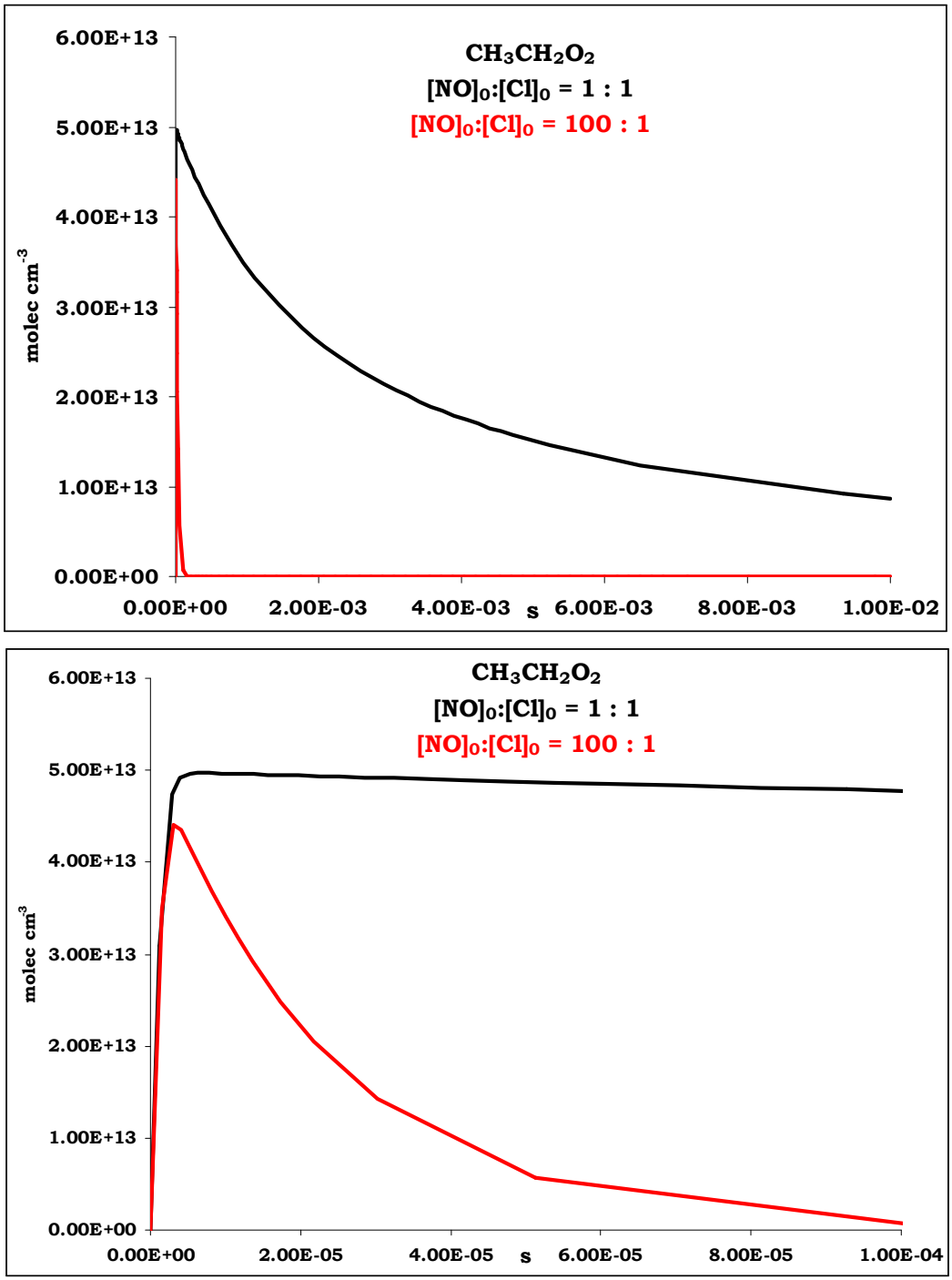

Figure 5.11. Concentrations of the ethyl peroxy radical using the kinetic model from Tables 5.2. The initial reactant concentrations are: $[C_2H_6]_0$ = 3 × 10^{16} molec cm^{-3} (1 Torr), $[Cl]_0$ = 5 × 10^{13} molec cm^{-3}, and $[O_2]_0$ = 50 × 3 × 10^{16} molec cm^{-3}. In black, $[NO]_0$:$[Cl]_0$ = 1, while in red, $[NO]_0$:$[Cl]_0$ = 100. The bottom plot looks at early times of the same simulation.

Kinetic experiments with HO_2

Determination of the rate of reaction between ethyl peroxy radical and HO_2 is more complex, as HO_2 has to be generated in the cell simultaneously. Three common methods for HO_2 production are:[64]

Source 1:

$Cl + CH_3OH \rightarrow CH_2OH + HCl$ (5.20 a)

$k_{298\,K}(Cl + CH_3OH) = 5.5 \times 10^{-11}\ cm^3\ molec^{-1}\ s^{-1}$ (5.20 b)

$CH_2OH + O_2 \rightarrow CH_2O + HO_2$ (5.21 a)

$k_{298\,K}(HCO + O_2) = 9.1 \times 10^{-12}\ cm^3\ molec^{-1}\ s^{-1}$ (5.21 b)

Source 2:

$Cl + H_2CO \rightarrow HCl + HCO$ (5.22 a)

$k_{298\,K}(Cl + H_2CO) = 7.3 \times 10^{-11}\ cm^3\ molec^{-1}\ s^{-1}$ (5.22 b)

$HCO + O_2 \rightarrow CO + HO_2$ (5.23 a)

$k_{298\,K}(HCO + O_2) = 5.2 \times 10^{-12}\ cm^3\ molec^{-1}\ s^{-1}$ (5.23 b)

Source 3:

$H_2O_2 + h\nu\ (248\ nm) \rightarrow 2\ HO_2$ (5.24 a)

with $\sigma_{248\,nm}(H_2O_2) = 9 \times 10^{-20}\ cm^2$ (5.24 b)

The first approach is the easiest to implement. The first overtone of the OH stretch of methanol (CH_3OH) is between 7000-7300 cm^{-1} region;[70] thus, the absorption is to the red of origin transitions of large peroxy radical absorptions in the NIR. Methanol however competes with ethane for the chlorine atoms. Thus, experiments can no longer be run under pseudo-first-order conditions.

$CH_3CH_2O_2 + HO_2 \rightarrow$ products (5.25 a)

$$-\frac{\partial[CH_3CH_2O_2]}{\partial t} = k[HO_2][CH_3CH_2O_2] \quad (5.25\ b)$$

Reactions in Table 5.3 were added to the kinetics model. The concentrations of both ethyl peroxy radical and HO_2 are shown in Fig. 5.12 with initial concentrations of reactants, ethane and methanol, at 1:1, 100:1, and 1:100 ratios. Measuring the decays of ethyl peroxy radical under the different conditions would confirm our control of HO_2 concentrations from source 1. An interesting comparison would be to also measure the HO_2 decays. The origin of the $\tilde{A} \leftarrow \tilde{X}$ transition of HO_2 is located 7029.688 cm^{-1},[77] within the scanning range of our pulsed CRDS apparatus. Contributions from methanol absorption should be effectively removed during subtraction of the photolysis scans (excimer on and off).

Kinetics model for Cl + ethane with HO_2	
Reaction formulas	**Rates of reaction at T = 298 K [cm^3 $molec^{-1}$ s^{-1}]**
$HO_2 + Cl \rightarrow HCl + O_2$	3.2×10^{-11}
$\rightarrow OH + ClO$	9.1×10^{-12}
$HO_2 + ClO \rightarrow HOCl + O_2$	5.6×10^{-12}

Table 5.3. Kinetics model for Cl + ethane with HO_2, in addition to the reactions included in Table 5.1 and Table 5.2. Rates of reaction from ref [64].

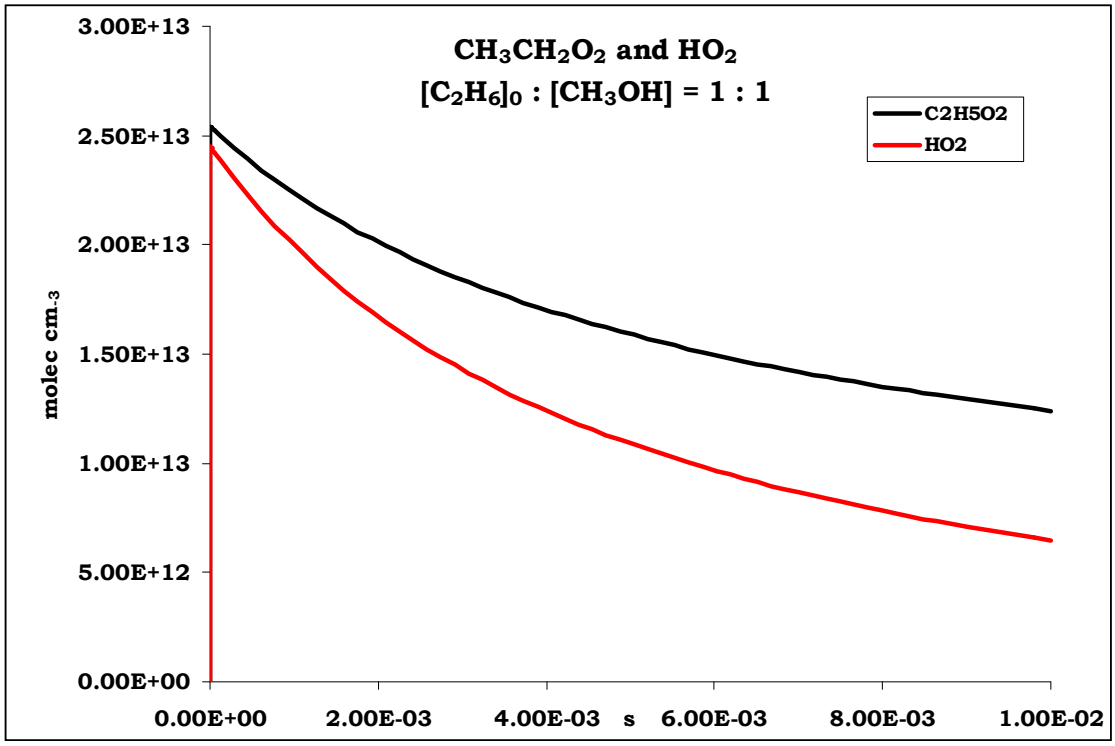
CH3CH2O2 and HO2
[C2H6]0 : [CH3OH] = 1 : 1
C2H5O2
HO2
molec cm-3
3.00E+13
2.50E+13
2.00E+13
1.50E+13
1.00E+13
5.00E+12
0.00E+00
0.00E+00
2.00E-03
4.00E-03
s
6.00E-03
8.00E-03
1.00E-02

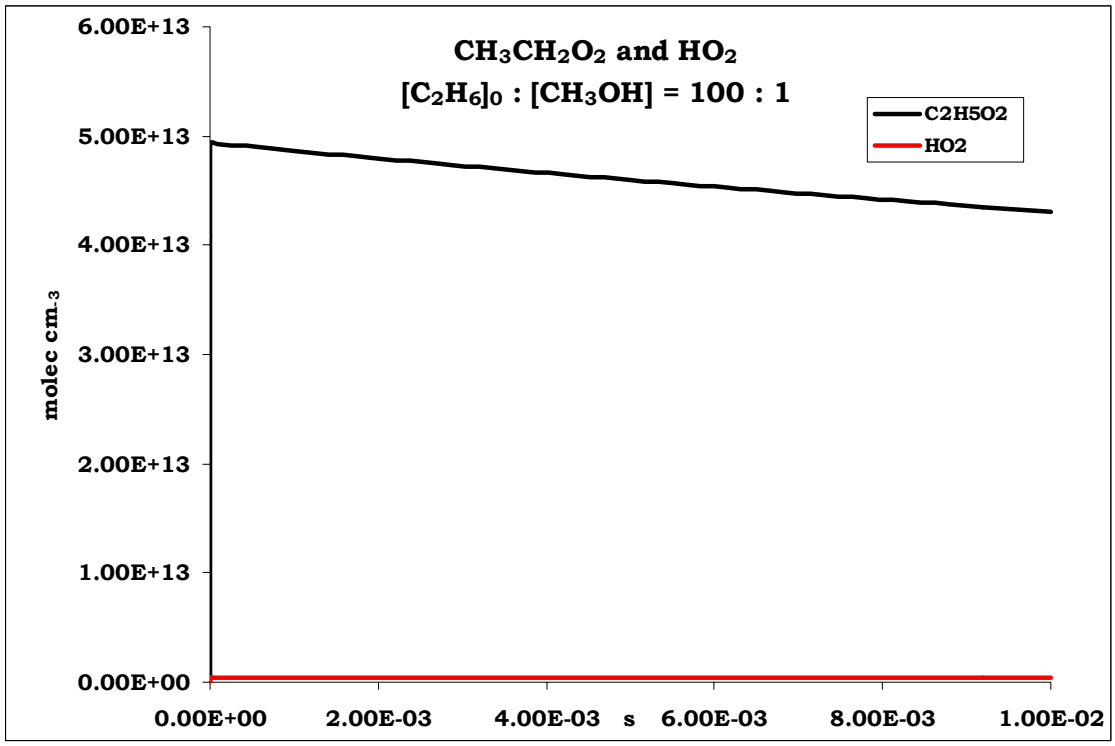
CH3CH2O2 and HO2
[C2H6]0 : [CH3OH] = 100 : 1
C2H5O2
HO2
molec cm-3
6.00E+13
5.00E+13
4.00E+13
3.00E+13
2.00E+13
1.00E+13
0.00E+00
0.00E+00
2.00E-03
4.00E-03
s
6.00E-03
8.00E-03
1.00E-02

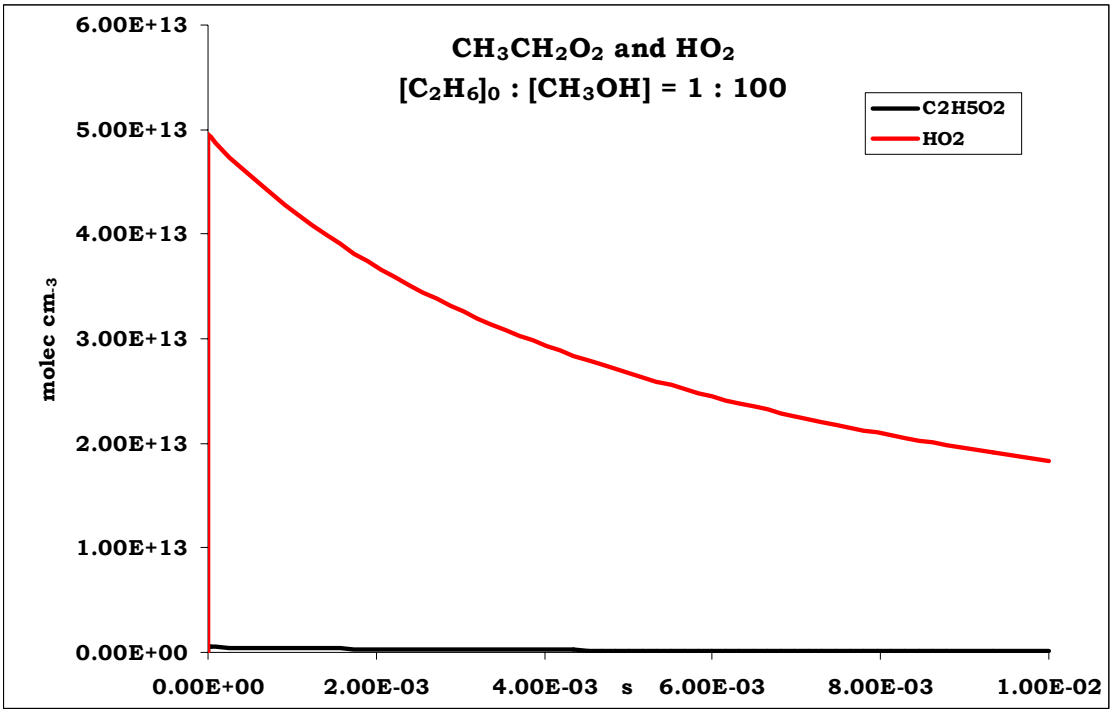

Figure 5.12. Concentrations of the ethyl peroxy radical and HO_2 using the kinetic model from Tables 5.3. The initial reactant concentrations are: $[C_2H_6]_0 = 3 \times 10^{16}$ molec cm^{-3} (~1 Torr), $[Cl]_0 = 5 \times 10^{13}$ molec cm^{-3}, and $[O_2]_0 = 50 \times 3 \times 10^{16}$ molec cm^{-3}. The ratio of the ethane and methanol reactants were varied: $[C_2H_6]_0$:$[CH_3OH]_0 = 1$ (top, on previous page), $[C_2H_6]_0$:$[CH_3OH]_0 = 100$ (middle), and $[C_2H_6]_0$:$[CH_3OH]_0 = 0.01$ (bottom). Note: for these simulations, $[NO]_0 = 0$.

If the chemical approach is unable to be well-quantified, we will try the other HO_2 sources. Formaldehyde (H_2CO) is difficult to use, as paraformaldehyde must be warmed carefully in a separate vessel to avoid oligomerization. Our group has experience using formaldehyde in other experiments.[78] Hydrogen peroxide (H_2O_2) is often available commercially as a 30% mixture of H_2O_2 and water. Concentrated H_2O_2 is explosive. Water, however, causes both spectral and chemical interference. We are in the process of exploring methods to safely collect concentrated H_2O_2.

5.4 Summary

We collected preliminary CRD spectra of the $\tilde{A} \leftarrow \tilde{X}$ transitions of Cl-isoprenyl and Cl-MBO232 peroxy radicals in the 7200-7700 cm^{-1} region. Neither species had ever been detected in the gas phase by absorption spectroscopy. The novel detection of the Cl-peroxy radicals provided groundwork for studies on the kinetics of Cl-peroxy radical species under high and low NO_x conditions. We outlined preliminary control experiments on the kinetics of ethyl peroxy radicals to prepare the apparatus and gas lines for kinetic studies of the Cl-peroxy radicals. As many of the reactions rates between Cl-peroxy radicals and atmospheric species have never been measured, these experiments will be highly useful for atmospheric modeling.

5.5 Afterword

We began with an examination of the chemical physics of the nitrate radical (NO_3) (Chapter 3) before exploring its role in the oxidation of VOCs in the atmosphere (Chapter 4). On one level, the chlorine (Cl) chemistry discussed in this chapter was a simple extension of the study of substituted peroxy radicals. The reaction pathways of Cl and NO_3 oxidation of alkenes are indeed parallel. The connection however between chlorine and nitrate radical is more complex. For example, the same dinitrogen pentaoxide (N_2O_5) that decomposes to NO_3 at night also reacts with chlorine ions to produce nitryl chloride ($ClNO_2$), the photolytic precursors of Cl atoms. Thus, nighttime or daytime, coastal or inland, the atmospheric networks are deeply intertwined. Understanding the chemistry of our atmosphere is understanding all the individual components of the network.

We discussed only a few but important pieces of the atmospheric puzzle in this work. The quality of the air, the climate of the Earth, and the effects on public health are all issues that will only continue to grow in the next century. We have both a scientific and societal responsibility to learn more about our atmosphere. It is the author's hope that others continue the work presented in the thesis and enjoy the same journey of learning that she had over the past years. Cheers!

5.5 References

(1) Finlayson-Pitts, B. J.; Pitts, J. N. *Chemistry of the Upper and Lower Atmosphere: Theory, Experiments, and Applications*; Academic Press, 1999.

(2) Finlayson-Pitts, B. J. *Chemical Reviews* **2003**, *103*, 4801.

(3) Graedel, T. E.; Keene, W. C. *Global Biogeochemical Cycles* **1995**, *9*, 47.

(4) Keene, W. C.; Khalil, M. A. K.; Erickson, D. J.; McCulloch, A.; Graedel, T. E.; Lobert, J. M.; Aucott, M. L.; Gong, S. L.; Harper, D. B.; Kleiman, G.; Midgley, P.; Moore, R. M.; Seuzaret, C.; Sturges, W. T.; Benkovitz, C. M.; Koropalov, V.; Barrie, L. A.; Li, Y. F. *Journal of Geophysical Research-Atmospheres* **1999**, *104*, 8429.

(5) Moldanova, J.; Ljungstrom, E. *Journal of Geophysical Research - Atmospheres* **2001**, *106*, 1271.

(6) Thomas, J. L.; Jimenez-Aranda, A.; Finlayson-Pitts, B. J.; Dabdub, D. *Journal of Physical Chemistry A* **2006**,*110*, 1859.

(7) Pszenny, A. A. P.; Keene, W. C.; Jacob, D. J.; Fan, S.; Maben, J. R.; Zetwo, M. P.; Springeryoung, M.; Galloway, J. N. *Geophysical Research Letters* **1993**, *20*, 699.

(8) Ghosal, S.; Brown, M. A.; Bluhm, H.; Krisch, M. J.; Salmeron, M.; Jungwirth, P.; Hemminger, J. C. *Journal of Physical Chemistry A* **2008**, *112*, 12378.

(9) Hoffman, R. C.; Gebel, M. E.; Fox, B. S.; Finlayson-Pitts, B. J. *Physical Chemistry Chemical Physics* **2003**, *5*, 1780.

(10) Leu, M. T.; Timonen, R. S.; Keyser, L. F.; Yung, Y. L. *Journal of Physical Chemistry* **1995**, *99*, 13203.

(11) Roberts, J. M.; Osthoff, H. D.; Brown, S. S.; Ravishankara, A. R. *Science* **2008**, *321*, 1059.

(12) Thornton, J. A.; Abbatt, J. P. D. *Journal of Physical Chemistry A* **2005**, *109*, 10004.

(13) Wingen, L. M.; Moskun, A. C.; Johnson, S. N.; Thomas, J. L.; Roeselova, M.; Tobias, D. J.; Kleinman, M. T.; Finlayson-Pitts, B. J. *Physical Chemistry Chemical Physics* **2008**, *10*, 5668.

(14) Knipping, E. M.; Lakin, M. J.; Foster, K. L.; Jungwirth, P.; Tobias, D. J.; Gerber, R. B.; Dabdub, D.; Finlayson-Pitts, B. J. *Science* **2000**, *288*, 301.

(15) Knipping, E. M.; Dabdub, D. *Environmental Science & Technology* **2003**, *37*, 275.

(16) Osthoff, H. D.; Roberts, J. M.; Ravishankara, A. R.; Williams, E. J.; Lerner, B. M.; Sommariva, R.; Bates, T. S.; Coffman, D.; Quinn, P. K.; Dibb, J. E.; Stark, H.; Burkholder, J. B.; Talukdar, R. K.; Meagher, J.; Fehsenfeld, F. C.; Brown, S. S. *Nature Geoscience* **2008**, *1*, 324.

(17) Thornton, J. A.; Kercher, J. P.; Riedel, T. P.; Wagner, N. L.; Cozic, J.; Holloway, J. S.; Dube, W. P.; Wolfe, G. M.; Quinn, P. K.; Middlebrook, A. M.; Alexander, B.; Brown, S. S. *Nature* **2010**, *464*, 271.

(18) von Glasow, R. *Nature* **2010**, *464*, 168.

(19) Brown, S. S.; Dube, W. P.; Fuchs, H.; Ryerson, T. B.; Wollny, A. G.; Brock, C. A.; Bahreini, R.; Middlebrook, A. M.; Neuman, J. A.; Atlas, E.; Roberts, J. M.; Osthoff, H. D.; Trainer, M.; Fehsenfeld, F. C.; Ravishankara, A. R. *Journal of Geophysical Research - Atmospheres* **2009**, *114*.

(20) Kercher, J. P.; Riedel, T. P.; Thornton, J. A. *Atmospheric Measurement Techniques* **2009**, *2*, 193.

(21) Chang, S. Y.; McDonald-Buller, E.; Kimura, Y.; Yarwood, G.; Neece, J.; Russell, M.; Tanaka, P.; Allen, D. *Atmospheric Environment* **2002**, *36*, 4991.

(22) Tanaka, P. L.; Oldfield, S.; Neece, J. D.; Mullins, C. B.; Allen, D. T. *Environmental Science & Technology* **2000**, *34*, 4470.

(23) Tanaka, P. L.; Riemer, D. D.; Chang, S. H.; Yarwood, G.; McDonald-Buller, E. C.; Apel, E. C.; Orlando, J. J.; Silva, P. J.; Jimenez, J. L.; Canagaratna, M. R.; Neece, J. D.; Mullins, C. B.; Allen, D. T. *Atmospheric Environment* **2003**, *37*, 1393.

(24) Aucott, M. L.; McCulloch, A.; Graedel, T. E.; Kleiman, G.; Midgley, P.; Li, Y. F. *Journal of Geophysical Research - Atmospheres* **1999**, *104*, 8405.

(25) McCulloch, A.; Aucott, M. L.; Benkovitz, C. M.; Graedel, T. E.; Kleiman, G.; Midgley, P. M.; Li, Y. F. *Journal of Geophysical Research - Atmospheres* **1999**, *104*, 8391.

(26) McCulloch, A.; Aucott, M. L.; Graedel, T. E.; Kleiman, G.; Midgley, P. M.; Li, Y. F. *Journal of Geophysical Research - Atmospheres* **1999**, *104*, 8417.

(27) Seinfeld, J. H.; Pandis, S. N. *Atmospheric Chemistry and Physics*; Wiley-Interscience, 1997.

(28) Lei, W. F.; Zhang, D.; Zhang, R. Y.; Molina, L. T.; Molina, M. J. *Chemical Physics Letters* **2002**, *357*, 45.

(29) Lei, W. F.; Zhang, R. Y.; Molina, L. T.; Molina, M. J. *Journal of Physical Chemistry A* **2002**, *106*, 6415.

(30) Ezell, M. J.; Wang, W. H.; Ezell, A. A.; Soskin, G.; Finlayson-Pitts, B. J. *Physical Chemistry Chemical Physics* **2002**, *4*, 5813.

(31) Riemer, D. D.; Apel, E. C.; Orlando, J. J.; Tyndall, G. S.; Brune, W. H.; Williams, E. J.; Lonneman, W. A.; Neece, J. D. *Journal of Atmospheric Chemistry* **2008**, *61*, 227.
(32) Orlando, J. J.; Tyndall, G. S.; Apel, E. C.; Riemer, D. D.; Paulson, S. E. *International Journal of Chemical Kinetics* **2003**, *35*, 334.
(33) Ceacero-Vega, A. A.; Ballesteros, B.; Albaladejo, J.; Bejan, I.; Barnes, I. *Chemical Physics Letters* **2009**, *484*, 10.
(34) Iwasaki, E.; Chiba, H.; Nakayama, T.; Matsumi, Y.; Wallington, T. J. *Chemical Physics Letters* **2010**, *494*, 174.
(35) Kaiser, E. W.; Wallington, T. J. *Chemical Physics Letters* **2011**, *501*, 187.
(36) Xing, J. H.; Takahashi, K.; Hurley, M. D.; Wallington, T. J. *Chemical Physics Letters* **2009**, *472*, 39.
(37) Andersen, M. P. S.; Nilsson, E. J. K.; Nielsen, O. J.; Johnson, M. S.; Hurley, M. D.; Wallington, T. J. *Journal of Photochemistry and Photobiology a-Chemistry* **2008**, *199*, 92.
(38) Kaiser, E. W.; Donahue, C. J.; Pala, I. R.; Wallington, T. J.; Hurley, M. D. *Journal of Physical Chemistry A* **2007**, *111*, 1286.
(39) Finlayson-Pitts, B. J.; Keoshian, C. J.; Buehler, B.; Ezell, A. A. *International Journal of Chemical Kinetics* **1999**, *31*, 491.
(40) Hsin, H. Y.; Elrod, M. J. *Journal of Physical Chemistry A* **2007**, *111*, 613.
(41) Patchen, A. K.; Pennino, M. J.; Elrod, M. J. *Journal of Physical Chemistry A* **2005**, *109*, 5865.
(42) Ragains, M. L.; FinlaysonPitts, B. J. *Journal of Physical Chemistry A* **1997**, *101*, 1509.
(43) Fan, J. W.; Zhang, R. Y. *Environmental Chemistry* **2004**, *1*, 140.
(44) Canosa-Mas, C. E.; Hutton-Squire, H. R.; King, M. D.; Stewart, D. J.; Thompson, K. C.; Wayne, R. P. *Journal of Atmospheric Chemistry* **1999**, *34*, 163.
(45) Fantechi, G.; Jensen, N. R.; Saastad, O.; Hjorth, J.; Peeters, J. *Journal of Atmospheric Chemistry* **1998**, *31*, 247.
(46) Stutz, J.; Ezell, M. J.; Ezell, A. A.; Finlayson-Pitts, B. J. *Journal of Physical Chemistry A* **1998**, *102*, 8510.
(47) Suh, I.; Zhang, R. Y. *Journal of Physical Chemistry A* **2000**, *104*, 6590.
(48) Timerghazin, Q. K.; Ariya, P. A. *Physical Chemistry Chemical Physics* **2001**, *3*, 3981.
(49) Wang, W. H.; Finlayson-Pitts, B. J. *Journal of Geophysical Research-Atmospheres* **2001**, *106*, 4939.

(50) Kesselmeier, J.; Staudt, M. *Journal of Atmospheric Chemistry* **1999**, *33*, 23.
(51) Atkinson, R.; Arey, J. *Atmospheric Environment* **2003**, *37*, S197.
(52) Goldan, P. D.; Kuster, W. C.; Fehsenfeld, F. C.; Montzka, S. A. *Geophysical Research Letters* **1993**, *20*, 1039.
(53) Schade, G. W.; Goldstein, A. H.; Gray, D. W.; Lerdau, M. T. *Atmospheric Environment* **2000**, *34*, 3535.
(54) Tarvainen, V.; Hakola, H.; Hellen, H.; Back, J.; Hari, P.; Kulmala, M. *Atmospheric Chemistry and Physics* **2005**, *5*, 989.
(55) Takahashi, K.; Xing, J. H.; Hurley, M. D.; Wallington, T. J. *Journal of Physical Chemistry A* **2010**, *114*, 4224.
(56) Rodriguez, A.; Rodriguez, D.; Soto, A.; Notario, A.; Aranda, A.; Diaz-De-Mera, Y.; Bravo, I. *Atmospheric Environment* **2007**, *41*, 4693.
(57) Ferronato, C.; Orlando, J. J.; Tyndall, G. S. *Journal of Geophysical Research - Atmospheres* **1998**, *103*, 25579.
(58) Chakir, A.; Brion, J.; Ganne, J. P.; Daumont, D. *Physical Chemistry Chemical Physics* **2003**, *5*, 2573.
(59) Biggs, P.; Canosa-Mas, C. E.; Percival, C. J.; Shallcross, D. E.; Wayne, R. P. *International Journal of Chemical Kinetics* **1999**, *31*, 433.
(60) Le Crane, I. P.; Villenave, E. *International Journal of Chemical Kinetics* **2006**, *38*, 276.
(61) Villenave, E.; Morozov, I.; Lesclaux, R. *Journal of Physical Chemistry A* **2000**, *104*, 9933.
(62) Deev, A., California Institute of Technology, 2005.
(63) Baklanov, A. V.; Krasnoperov, L. N. *Journal of Physical Chemistry A* **2001**, *105*, 97.
(64) Sander, S. P.; Friedl, R. R.; Golden, D. M.; Kurylo, M.; Moortgat, G. K.; Wine, P. H.; Ravishankara, A. R.; Kolb, C. E.; Molina, M. J.; Finlayson-Pitts, B. J.; Huie, R. E.; Orkin, V. L. *Chemical Kinetics and Photochemical Data for Use in Atmospheric Studies, Evaluation No. 15,* 2006.
(65) Rupper, P.; Sharp, E. N.; Tarczay, G.; Miller, T. A. *J. Phys. Chem. A* **2007**, *111*, 832.
(66) Just, G. M. P.; McCoy, A. B.; Miller, T. A. *Journal of Chemical Physics* **2007**, *127*, 044310/1.
(67) Sharp, E. N.; Rupper, P.; Miller, T. A. *Phys. Chem. Chem. Phys.* **2008**, *10*, 3955.
(68) Melnik, D.; Chhantyal-Pun, R.; Miller, T. A. *Journal of Physical Chemistry A* **2010**, *114*, 11583.

(69) Sharp, E. N.; Rupper, P.; Miller, T. A. *Journal of Physical Chemistry A* **2008**, *112*, 1445.
(70) Sharpe, S. W.; Johnson, T. J.; Sams, R. L.; Chu, P. M.; Rhoderick, G. C.; Johnson, P. A. *Applied Spectroscopy* **2004**, *58*, 1452.
(71) King, M. D.; Thompson, K. C. *Atmospheric Environment* **2003**, *37*, 4517.
(72) Kosmas, A. M.; Salta, Z.; Lesar, A. *Journal of Physical Chemistry A* **2009**, *113*, 3545.
(73) Atkinson, R.; Baulch, D. L.; Cox, R. A.; Crowley, J. N.; Hampson, R. F.; Hynes, R. G.; Jenkin, M. E.; Rossi, M. J.; Troe, J. *Atmospheric Chemistry and Physics* **2004**, *4*, 1461.
(74) Ianni, J. C. 2011.
(75) Noell, A. C.; Alconcel, L. S.; Robichaud, D. J.; Okumura, M.; Sander, S. P. *Journal of Physical Chemistry A* **2010**, *114*, 6983.
(76) Atkinson, D. B.; Hudgens, J. W. *Journal of Physical Chemistry A* **1997**, *101*, 3901.
(77) Fink, E. H.; Ramsay, D. A. *Journal of Molecular Spectroscopy* **2002**, *216*, 322.
(78) Mollner, A., *Ph. D. Thesis,* California Institute of Technology, 2007.